Available online at www.sciencedirect.com
SCIENCE DIRECT®
Journal of Computational Physics 184 (2003) 381–405
JOURNAL OF COMPUTATIONAL PHYSICS
www.elsevier.com/locate/jcp

Force-coupling method for particulate two-phase flow: Stokes flow

Sune Lomholt [a,1], Martin R. Maxey [b,*]

[a] *Risø National Laboratory, Roskilde, Denmark*
[b] *Division of Applied Mathematics, Brown University, 182 George Street, Box F, Providence, RI 02912, USA*

Received 9 August 2001; accepted 30 September 2002

Abstract

In this paper we describe a force-coupling method for particle dynamics in fluid flows. The general principles of the model are described and it is tested on three different Stokes flow problems; a single isolated sphere, a pair of otherwise isolated spheres, and a single sphere in a channel. For sphere to sphere or sphere to wall distances larger than 1/4 of the sphere radius the force-coupling results compared well with analytical and accurate numerical values. For smaller distances the results agree qualitatively, but lubrication effects are not included and this leads to a quantitative discrepancy.

Keywords: Particulate flow; Stokes flow; Two-phase flow; Force-coupling

1. Introduction

Over the last decade, it has become possible to develop micro-electromechanical systems (MEMS) for applications in chemical, biochemical or biomedical analysis. These devices combine electrical and mechanical components on a small silicon or polymer chip and among their possible uses are the sorting or analysis of cells and particles, and the separation of particles from a fluid sample. The general context of these applications is reviewed by Ho and Tai [1] and a specific example of a particle separation device is described by Lomholt et al. [2]. An important aspect in the design of these devices is to be able to determine the motion of particles in the liquid flow as they move through possibly complex geometries under a range of conditions for Reynolds number, particle size, concentration, and body forces acting on the particle. Similar issues arise too in more traditional areas of dispersed two-phase flow where solid particles are transported in a liquid and may be settling under gravity or subject to a shear flow.

* Corresponding author. Tel.: 1-401-863-1482; fax: 1-401-863-2722.
E-mail address: maxey@cfm.brown.edu (M.R. Maxey).
[1] Present address: OFS Fitel Denmark I/S, Priorparken 680, 2605 Brøndby, Denmark.

0021-9991/02/$ - see front matter
PII: S0021-9991(02)00021-9

One standard approach to determining the unsteady motion of a small rigid particle in a viscous fluid is to apply the Basset–Boussinesq–Oseen theory, see for example [3]. This specifies an equation of motion for each particle based on the local ambient flow. However, this method is limited to very low particle Reynolds numbers and to isolated, small particles that are well separated from boundaries or each other. Efforts have been made by Lovalenti and Brady [4], Lawrence and Mei [5] and others to extend the range of application of this approach but many of the basic limitations still remain.

In confined flows, or dispersed two-phase flows where the mass-fraction of the particles is significant, the fully coupled dynamics of the fluid motion and the particle motion need to be considered. In the context of steady, low Reynolds number, Stokes flows a variety of methods are now well-established such as Stokesian dynamics described by Brady and Bossis [6], multipole methods as described for example by Happel and Brenner [7], Mazur and Van Saarloos [8] or Kim and Karrila [9], or boundary element methods. Specific applications of the multipole method for particle sedimentation are given by Ladd [10], [11], and Sangani and Mo [12]. Improvements to the Stokesian dynamics algorithm have been made recently by Ichiki and Brady [13] and by Sierou and Brady [14].

For more general flow conditions the full Navier–Stokes equations are solved numerically as in the finite element computations of Hu [15] and Johnson and Tezduyar [16]. In these, the full no-slip boundary conditions are applied on each particle and the fluid forces evaluated to determine the particle motion in the flow. The underlying finite elements deform in an arbitrary Lagrangian–Eulerian (ALE) scheme as the particles move through the fluid. The elements are then periodically remeshed to maintain numerical resolution. This approach provides good accuracy but is computationally intensive. Alternatively, Glowinski et al. [17] and Patankar et al. [18] employ a fictitious domain method with a fixed numerical mesh and impose a distributed Langrange multiplier (DLM) to force the fluid inside the particle to respond as a rigid body. This scheme too may become computationally intensive as more constraints are imposed. Unverdi and Tryggvason [19] similarly use a fixed numerical mesh in a front-tracking scheme that has been very successfully used to simulate the motion of deforming drops and bubbles in liquids. In these higher resolution methods up to 18 grid points, for a uniform mesh, may be needed per particle diameter to properly resolve the flow details.

In this paper we describe an approximate, yet effective method for calculating these particle-flow interactions based on a force-coupling procedure. The method is outlined in Maxey et al. [20], and in more detail in Maxey and Patel [21] for the context of Stokes flows. The method is conceptually similar to Stokesian dynamics but is applicable to both Stokes and finite Reynolds number flows. The basic approach is to represent the presence of each particle in the flow by a low-order expansion of finite-valued, force multipoles applied as a distributed body force on the flow. Fluid fills the whole domain, including the volume occupied by the particles, and the Navier–Stokes equations are solved throughout the domain on a fixed numerical mesh. Unlike traditional multipole methods or Stokesian dynamics, no singularities are encountered and no special consideration is needed for the self-induced flow of a particle. Indeed such flows allow us to incorporate directly the finite-size of the particle and the length scale of the force distribution is directly related to the radius of the particle. This scheme requires only about 4–6 grid points per particle diameter on a uniform mesh, and is straightforward to implement with existing codes for solving the Navier–Stokes equations. The velocity of each particle is found from the local fluid velocity and from this the Lagrangian motion of the particle is calculated. The disadvantage of the method is that the flow close to the surface of each particle is not resolved and there are limitations at present on the accuracy of close-particle interactions in the flow. Beyond the issue of numerical simulations, the method further provides a basis for developing theoretical models of dispersed two-phase flows and for simplifying the description of these systems.

The purpose of this paper is to extend the force-coupling method as described in Maxey and Patel [21] for periodic domains to include higher-order effects through the introduction of force dipole terms and to extend it to bounded domains. These terms are needed for near interactions between particles, interactions

with wall boundaries, representing shear flow effects and determining the rotation rate of particles. The extended force-coupling method is then tested for several problems including the interaction of two particles in an open flow, a single spherical particle moving in a wall-bounded channel, or a particle in a Poiseuille flow. The theory and results are developed in the context of Stokes flow, and compared to established results. The method has been successfully applied to finite Reynolds number flows by Dent [22], Lomholt [23], and has been compared with data from laboratory experiments for finite Reynolds number conditions by Lomholt et al. [24].

2. The force-coupling method – general principles

The key elements of the approximate force-coupling method (FCM) for dispersed two-phase flow are as follows. The effect of the particles on the fluid phase are represented by a localized body force $\mathbf{f}(\mathbf{x},t)$ that transmits to the fluid the resultant force of the particles on the flow. The equations for fluid motion are applied to the whole domain, including the volume occupied by the particles, so the fluid velocity field $\mathbf{u}(\mathbf{x},t)$ satisfies

$$\rho\frac{\mathrm{D}\mathbf{u}}{\mathrm{D}t} = -\nabla p + \mu\nabla^2\mathbf{u} + \mathbf{f}(\mathbf{x},t), \tag{1}$$

where ρ,μ are the fluid density and viscosity respectively and p is the pressure. In addition there is the constraint of incompressible flow

$$\nabla\cdot\mathbf{u} = 0. \tag{2}$$

In the initial version of the force-coupling method a force monopole term alone is specified and

$$\mathbf{f}(\mathbf{x},t) = \sum_{n=1}^{N}\mathbf{F}^{(n)}\Delta\big(\mathbf{x}-\mathbf{Y}^{(n)}(t)\big), \tag{3}$$

where $\mathbf{Y}^{(n)}$ is the position of the nth spherical particle and $\mathbf{F}^{(n)}$ is the force this exerts on the fluid. The localized force distribution for each particle is determined by the function $\Delta(\mathbf{x})$ which is chosen as a Gaussian function

$$\Delta(\mathbf{x}) = (2\pi\sigma^2)^{-3/2}\exp\left(-\frac{\mathbf{x}^2}{2\sigma^2}\right), \tag{4}$$

and the length scale σ is set in terms of the particle radius a as

$$\frac{a}{\sigma} = \sqrt{\pi}. \tag{5}$$

The velocity of each particle $\mathbf{V}^{(n)}(t)$ is found by forming a local average of the fluid velocity over the region occupied by the particle as

$$\mathbf{V}^{(n)}(t) = \int\mathbf{u}(\mathbf{x},t)\Delta\big(\mathbf{x}-\mathbf{Y}^{(n)}(t)\big)\,\mathrm{d}^3\mathbf{x}. \tag{6}$$

The value of the ratio a/σ given in (5) is determined by matching the induced particle velocity with the Stokes settling velocity for an isolated particle settling under gravity in the limit of zero Reynolds number. Discussions on how to determine the particle velocity are given in Maxey et al. [20] and Maxey and Patel [21].

An important aspect of the model is the overall kinetic energy budget for the flow. The total fluid kinetic energy is found by forming the scalar product of the fluid momentum Eq. (1) with $\mathbf{u}(\mathbf{x},t)$ and integrating this over the whole domain, including the volume occupied by the particle phase. The resulting terms are the usual rate of change of fluid kinetic energy, the transport of kinetic energy in or out of the domain, the rate of work done by the fluid stresses on the boundary of the domain, the viscous dissipation and the rate of work by the particulate phase on the fluid which is then

$$\int \mathbf{u}\cdot\mathbf{f}\,\mathrm{d}^3\mathbf{x}. \tag{7}$$

Inserting $\mathbf{f}$ from (3) this rate of work by the particulate phase is equal to

$$\sum_{n=1}^{N}\int \mathbf{u}(\mathbf{x},t)\cdot\mathbf{F}^{(n)}\Delta\big(\mathbf{x}-\mathbf{Y}^{(n)}\big)\,\mathrm{d}^3\mathbf{x}, \tag{8}$$

which in turn is equal to

$$\sum_{n=1}^{N}\mathbf{F}^{(n)}\cdot\mathbf{V}^{(n)}. \tag{9}$$

The above expression is the sum of the individual contributions of each particle to the rate of work, namely the scalar product of particle velocity with the resultant force the particle exerts on the fluid. The total rate of viscous dissipation of kinetic energy is found by integrating the local dissipation rate over the whole domain, including the volume occupied by the particles, as

$$\int 2\mu e_{ij}e_{ij}\,\mathrm{d}^3\mathbf{x}, \tag{10}$$

where e_{ij} is the local rate of strain. Consequently, when the particle velocity is found using (6) the kinetic energy budget in the model is self-consistent.

With the force-coupling method we do not attempt to match the exact no-slip boundary conditions on the surface of each particle nor does the model reproduce the full flow structure close to each particle. Instead the flow is locally smoothed out, or spatially filtered. However, the flow representation away from the surface of a particle and the interaction of particles through the flows they generate are adequately resolved. In order to improve the flow representation the force-coupling model may be extended to include force dipoles in addition to the monopoles in (3) so that

$$f_i(\mathbf{x},t)=\sum_{n=1}^{N}\left\{F_i^{(n)}\Delta\big(\mathbf{x}-\mathbf{Y}^{(n)}(t)\big)+G_{ij}^{(n)}\frac{\partial}{\partial x_j}\Delta'\big(\mathbf{x}-\mathbf{Y}^{(n)}(t)\big)\right\}. \tag{11}$$

The function $\Delta'(\mathbf{x})$ is also a Gaussian as in (4) but the length scale is instead σ' and differs from the length scale for the monopole term. In a standard multipole expansion a single distribution function and length scale would be used with σ chosen to be small compared to the particle radius [21]. With the force-coupling method the length scales are comparable to the particle size and are used as parameters in the model.

The dipole coefficient $G_{ij}^{(n)}$ is related to the moment of forces acting on the fluid and it consists of a symmetric part and an anti-symmetric part. The anti-symmetric part corresponds to a torque. For a single particle at the origin the torque density associated with the force distribution is $\mathbf{x}\times\mathbf{f}$ and the resultant torque on the fluid is

$$T_i=\int \epsilon_{ijk}x_j\left\{F_k\Delta(\mathbf{x})+G_{km}\frac{\partial}{\partial x_m}\Delta'(\mathbf{x})\right\}\mathrm{d}^3\mathbf{x}, \tag{12}$$

integrated over the whole domain. The monopole term produces no torque so the torque from the particle on the fluid is

$$T_i = \epsilon_{ijk} G_{jk}. \tag{13}$$

The rate of work on the fluid by an applied torque $\mathbf{T}$ is $\mathbf{T} \cdot \mathbf{\Omega}$, where $\mathbf{\Omega}$ is the induced rotation of the spherical particle. As before we may evaluate the rate of work on the fluid (7) by the force distribution $\mathbf{f}(\mathbf{x}, t)$ and the contribution from the additional force dipole term in general is

$$\int u_i(\mathbf{x}, t) G_{ij} \frac{\partial}{\partial x_j} \Delta'(\mathbf{x}) \, \mathrm{d}^3\mathbf{x}. \tag{14}$$

The anti-symmetric part of the dipole term is equal to $\frac{1}{2}\epsilon_{ijk} T_k$ (from (13)) and the rate of work by this anti-symmetric part is equal to

$$-\frac{1}{2}\epsilon_{ijk} T_k \int \frac{\partial u_i}{\partial x_j} \Delta'(\mathbf{x}) \, \mathrm{d}^3\mathbf{x}. \tag{15}$$

This matches the expected value $\mathbf{T} \cdot \mathbf{\Omega}$ provided the angular velocity of the particle is evaluated from the local fluid vorticity $\boldsymbol{\omega}$ as

$$\mathbf{\Omega} = \frac{1}{2} \int \boldsymbol{\omega}(\mathbf{x}, t) \Delta'(\mathbf{x}) \, \mathrm{d}^3\mathbf{x}. \tag{16}$$

The symmetric component of the dipole coefficient G_{ij} corresponds to a stresslet acting on the fluid. This is purely an internal force term acting between the fluid and particle phases, and arises from the fact that the particle is a rigid body. No net work is done and the contribution to the total rate of work is zero. In other words the components of the symmetric part of G_{ij} are chosen so that the constraint

$$\int \frac{1}{2} \left(\frac{\partial u_i}{\partial x_j} + \frac{\partial u_j}{\partial x_i} \right) \Delta'(\mathbf{x} - \mathbf{Y}) \, \mathrm{d}^3\mathbf{x} = 0 \tag{17}$$

is satisfied for each particle. This states that the locally averaged fluid rate of strain for the volume occupied by a particle is zero.

Hence, when the force-coupling method is extended with the force dipole terms, choosing the angular velocity of the particles as defined by (16) and imposing the constraint (17) ensure that a self-consistent kinetic energy budget is maintained.

3. Isolated Stokes particle

The extended force-coupling model, with both monopole and dipole terms, is first applied to the motion of a single isolated sphere moving in a low Reynolds number Stokes flow. In a viscous Stokes flow the fluid inertia is negligible compared to the viscous stresses. The corresponding form of the momentum Eq. (1) is

$$0 = -\nabla p + \mu \nabla^2 \mathbf{u} + \mathbf{f}(\mathbf{x}, t). \tag{18}$$

The inertia of the particles is neglected too and so the force $\mathbf{F}$ of a particle on the fluid is equal to the resultant external force on the particle, such as the force due to gravity in the context of gravitational settling in a suspension. In Maxey and Patel [21], the force-coupling model for Stokes flow was derived for the simple force monopole term in (3). The Stokes flow induced by the force monopole $\mathbf{F}\Delta(\mathbf{x})$ for a single isolated particle at the origin is

$$u_i = S_{ij}(\mathbf{x})F_j, \tag{19a}$$

$$S_{ij} = A(r)\delta_{ij} + B(r)x_i x_j, \tag{19b}$$

where $r = |\mathbf{x}|$ and

$$A(r) = \frac{1}{8\pi\mu r}\left[\left(1+\frac{\sigma^2}{r^2}\right)\mathrm{erf}\left(\frac{r}{\sigma\sqrt{2}}\right) - \frac{2\sigma}{r}(2\pi)^{-1/2}\exp\left(-\frac{r^2}{2\sigma^2}\right)\right], \tag{20a}$$

$$B(r) = \frac{1}{8\pi\mu r^3}\left[\left(1-\frac{3\sigma^2}{r^2}\right)\mathrm{erf}\left(\frac{r}{\sigma\sqrt{2}}\right) + \frac{6\sigma}{r}(2\pi)^{-1/2}\exp\left(-\frac{r^2}{2\sigma^2}\right)\right]. \tag{20b}$$

Fig. 1 shows profiles along the x_1 and x_2 axis of the fluid velocity u_1 obtained from (19a) for the case of a sphere moving with the Stokes settling velocity W in the x_1 direction. Clearly the solution (19a) agrees well with the Stokes solution for distances $r/a > 1.25$.

Since the equations for Stokes flow are linear the flow induced by the force dipole in (11) may be obtained by differentiating the result (19a) with respect to $\mathbf{x}$. The Fourier transform of the flow field due to the force dipole of a single isolated particle at the origin is given by the solution of (18) as

$$\widehat{u}_i = (\mu k^2)^{-1}[\delta_{ij} - k_i k_j/k^2]ik_m\widehat{\Delta}'(\mathbf{k})G_{jm}. \tag{21}$$

The flow field is then

$$u_i = R_{ijk}(\mathbf{x})G_{jk}, \tag{22a}$$

$$R_{ijk} = \frac{\mathrm{d}A'}{\mathrm{d}r}\delta_{ij}x_k/r + B'(r)(\delta_{ik}x_j + \delta_{jk}x_i) + \frac{\mathrm{d}B'}{\mathrm{d}r}x_i x_j x_k/r, \tag{22b}$$

and the functions $A'(r)$ and $B'(r)$ are based on (20a) and (20b) with the length scale σ',

$$\frac{\mathrm{d}A'}{\mathrm{d}r} = -\frac{1}{8\pi\mu r^2}\left[\left(1+\frac{3\sigma'^2}{r^2}\right)\mathrm{erf}\left(\frac{r}{\sigma'\sqrt{2}}\right) - \left(\frac{4r}{\sigma'} + \frac{6\sigma'}{r}\right)(2\pi)^{-1/2}\exp\left(-\frac{r^2}{2\sigma'^2}\right)\right], \tag{23a}$$

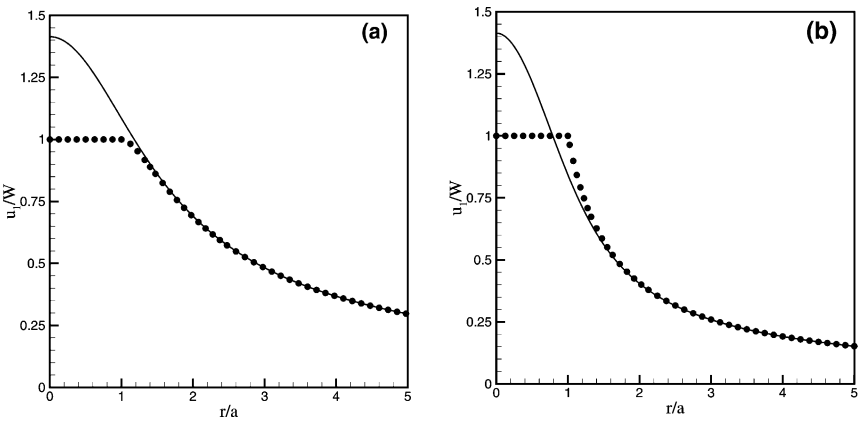

Fig. 1. Profiles of the u_1 fluid velocity along the x_1-axis (a) and the x_2-axis (b) for an isolated sphere of radius a moving with velocity W in positive x_1-direction as given by the force-coupling result (19a). The Stokes solution is shown as • and the FCM result as the line.

$$\frac{\mathrm{d}B'}{\mathrm{d}r} = -\frac{1}{8\pi\mu r^4}\left[\left(3-\frac{15\sigma'^2}{r^2}\right)\mathrm{erf}\left(\frac{r}{\sigma'\sqrt{2}}\right)+\left(\frac{4r}{\sigma'}+\frac{30\sigma'}{r}\right)(2\pi)^{-1/2}\exp\left(-\frac{r^2}{2\sigma'^2}\right)\right]. \tag{23b}$$

The local, volume-averaged velocity gradient for a single, isolated particle at the origin given as

$$\widetilde{\Gamma}_{ij} = \int \frac{\partial u_i}{\partial x_j}\Delta'(\mathbf{x})\,\mathrm{d}^3\mathbf{x}, \tag{24}$$

may be related directly to the dipole coefficient G_{ij}. The explicit relation is found from the Fourier transform (21) of the dipole flow field,

$$\widetilde{\Gamma}_{ij} = -G_{km}(2\pi)^{-3}\int\left[\delta_{ik}-\frac{k_ik_k}{k^2}\right]\frac{k_mk_j}{\mu k^2}\exp(-k^2\sigma'^2)\,\mathrm{d}^3\mathbf{k}. \tag{25}$$

The local volume-averages, such as (6) or (17) and (24), are convolution integrals and these correspond to a spatial filter in a Fourier representation. The force monopole has no effect on $\widetilde{\Gamma}_{ij}$ and the above relationship to G_{km} is isotropic so that for some constants α,β,γ the value of $\widetilde{\Gamma}_{ij}$ is

$$\widetilde{\Gamma}_{ij} = (\alpha\delta_{ij}\delta_{km}+\beta\delta_{ik}\delta_{jm}+\gamma\delta_{im}\delta_{jk})G_{km}. \tag{26}$$

From the symmetry of (25) in the indices i,k and j,m it follows that

$$\alpha = \gamma \tag{27}$$

and as the flow is incompressible

$$3\alpha+\beta+\gamma = 0. \tag{28}$$

As a result the average velocity gradient is

$$\widetilde{\Gamma}_{ij} = -3\alpha\left(G_{ij}-\frac{1}{3}\delta_{ij}G_{kk}\right)-\alpha(G_{ij}-G_{ji}). \tag{29}$$

A sum over both pairs of indices then yields from (25) the result

$$3\alpha+9\beta+3\gamma = -\left(4\mu\pi^{3/2}\sigma'^3\right)^{-1} \tag{30}$$

so that

$$\alpha = \left(120\mu\pi^{3/2}\sigma'^3\right)^{-1}. \tag{31}$$

As we will show below in Section 3.1 the appropriate choice for the length scale σ' is

$$\frac{a}{\sigma'} = \left(6\sqrt{\pi}\right)^{1/3} \tag{32}$$

or a/σ' is approximately 2.20. The local, volume-averaged velocity gradient is then

$$\widetilde{\Gamma}_{ij} = -\frac{3}{20\pi\mu a^3}\left(G_{ij}-\frac{1}{3}\delta_{ij}G_{kk}\right)-\frac{1}{20\pi\mu a^3}\left(G_{ij}-G_{ji}\right), \tag{33}$$

in agreement with standard results of Stokes flow as illustrated in the following sections.

3.1. Simple torque

An isolated particle subject to an applied torque $\mathbf{T}$ will rotate with an angular velocity $\mathbf{\Omega}$, which is given by the standard relation [7]

$$\mathbf{T} = 8\pi\mu a^3\mathbf{\Omega}. \tag{34}$$

The Stokes flow for the region outside the sphere is

$$\mathbf{u} = (8\pi\mu r^3)^{-1}(\mathbf{T}\times\mathbf{x}). \tag{35}$$

This satisfies the no-slip boundary condition on the surface of the particle and the fluid velocity there is $\mathbf{\Omega}\times\mathbf{x}$. The corresponding result of the force-coupling model, from (22a) to (23b), is

$$\mathbf{u} = (8\pi\mu r^3)^{-1}(\mathbf{T}\times\mathbf{x})\left[\operatorname{erf}\left(\frac{r}{\sigma'\sqrt{2}}\right) - \frac{r}{\sigma'}\left(\frac{2}{\pi}\right)^{1/2}\exp\left(-\frac{r^2}{2\sigma'^2}\right)\right] \tag{36}$$

with the dipole coefficient G_{ij} equal to $\frac{1}{2}\epsilon_{ijk}T_k$. Clearly these results for the flow match at points away from sphere, where the expression in the square brackets goes to one. In Fig. 2 the azimuthal velocity component given by the force-coupling method result (36) is compared to the exact result (35). As for the translating sphere in Fig. 1 the results agree well for distances $r/a > 1.25$.

For a given torque or dipole coefficient the force-coupling method specifies the angular velocity of the particle from (16), which in terms of the locally averaged velocity gradient is

$$\Omega_i = \frac{1}{2}\epsilon_{ijk}\widetilde{\Gamma}_{jk}. \tag{37}$$

Combining with (34) this may be written in terms of the anti-symmetric dipole coefficient as

$$\Omega_i = \frac{5}{2}\alpha\epsilon_{ijk}G_{jk}, \tag{38}$$

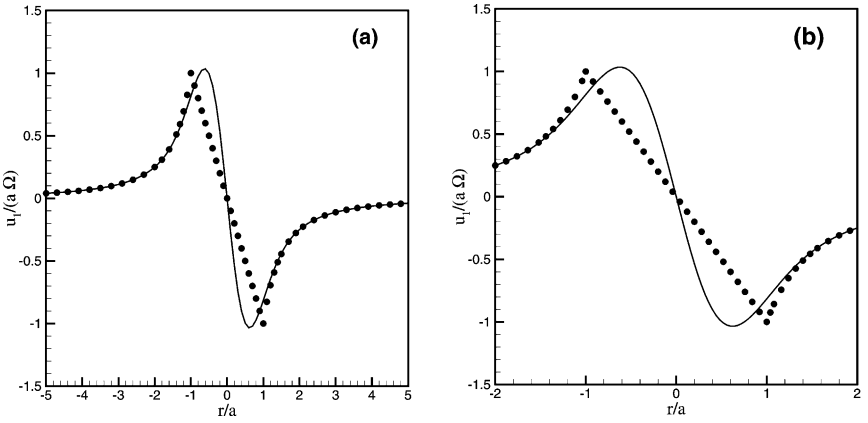

Fig. 2. Profile of the u_1 fluid velocity along the x_2-axis for an isolated sphere of radius a rotating with angular velocity Ω as given by the force-coupling result (36). The Stokes solution is shown as • and the FCM result as the line. (a) shows the long range agreement and (b) shows the agreement near the sphere surface.

or

$$\mathbf{\Omega} = \left(48\mu\pi^{3/2}\sigma'^3\right)^{-1}\mathbf{T}, \tag{39}$$

substituting the value of α from (31). Matching the angular velocity from the force-coupling method with angular velocity from the Stokes solution by equating (39) with (34) then gives the appropriate value of the ratio a/σ' for the dipole term and this is equal to that given in (32).

3.2. Uniform straining flow

An isolated rigid particle placed in a uniform external straining flow $u_i = E_{ij}x_j$ generates a local disturbance flow corresponding to a symmetric stresslet G_{ij} and a higher order degenerate force octapole so as to satisfy the no-slip boundary conditions on the surface of the spherical particle. The exact result for this induced Stokes flow is [9]

$$u_i = -\frac{3}{8\pi\mu r^5}x_i x_j x_k G_{jk} + \frac{3a^2}{40\pi\mu r^7}(5x_i x_j x_k - 2r^2\delta_{ij}x_k)G_{jk} \tag{40}$$

and the stresslet is

$$G_{ij} = \frac{20}{3}\pi\mu a^3 E_{ij}. \tag{41}$$

This stresslet has zero trace as the flow is incompressible.

The force-coupling method will also give rise to a stresslet to ensure that the locally volume-averaged rate of strain for the particle is zero, according to the condition (17). The flow induced by a symmetric, traceless stresslet G_{ij} according to the force-coupling model is from (22a) to (23b)

$$\begin{aligned} u_i = & -\frac{3}{8\pi\mu r^5}x_i x_j x_k G_{jk}\mathrm{erf}\left(\frac{r}{\sigma'\sqrt{2}}\right) + \frac{3\sigma'^2}{8\pi\mu r^7}\mathrm{erf}\left(\frac{r}{\sigma'\sqrt{2}}\right)(5x_i x_j x_k - 2r^2\delta_{ij}x_k)G_{jk} + (8\pi\mu r^4\sigma')^{-1}(2\pi)^{-1/2} \\ & \times \exp\left(-\frac{r^2}{2\sigma'^2}\right)\left\{4\left(r^2\delta_{ij}x_k - x_i x_j x_k\right) + \frac{6\sigma'^2}{r^2}(2r^2\delta_{ij}x_k - 5x_i x_j x_k)\right\}G_{jk}. \end{aligned} \tag{42}$$

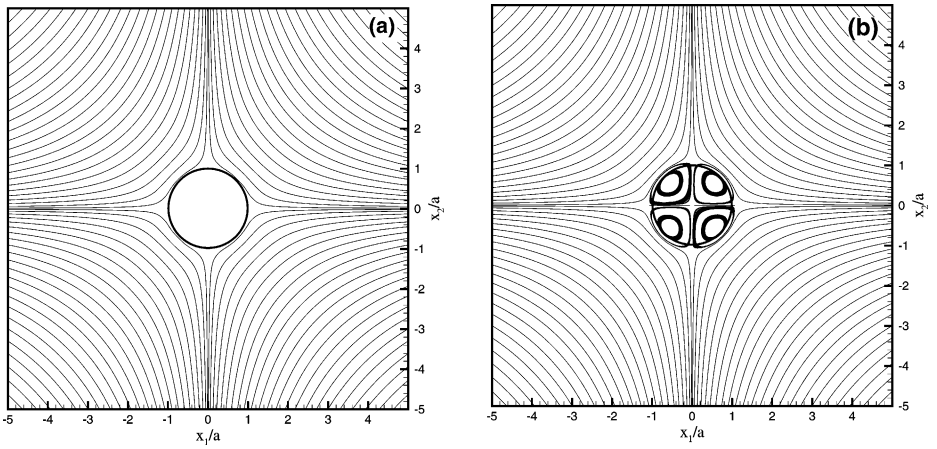

Fig. 3. Streamlines for a sphere in a uniform straining flow $u_1 = x_1$, $u_2 = -x_2$, and $u_3 = 0$. The streamlines are shown in the plane $x_3 = 0$. (a) shows the exact Stokes solution and (b) shows the approximate force-coupling solution.

The local volume-averaged rate of strain of this flow is given by (29) and if G_{ij} is symmetric and traceless then

$$\widetilde{\Gamma}_{ij} = -3\alpha G_{ij}. \tag{43}$$

With α given by (31) and the ratio a/σ' set by (32) then (43) implies that

$$\widetilde{\Gamma}_{ij} = -\frac{3}{20\pi\mu a^3} G_{ij}. \tag{44}$$

This is in agreement with the exact Stokes result (41). The force dipole creates a local velocity gradient to cancel the imposed external rate of strain E_{ij} and so satisfy the constraint (17).

The first two terms of the flow field (42) correspond to a combination of a pure stresslet flow and a degenerate force octapole sufficiently far from the particle center that the error function coefficient is approximately equal to one. The other terms in (42) decrease rapidly away from the particle center. The coefficient for the octapole term in (42) is $3\sigma'^2/8\pi\mu$ compared to $3a^2/40\pi\mu$ in the result for the exact Stokes flow (40). The ratio of these coefficients is $a^2/5\sigma'^2$ and they are approximately equal to within 3%.

Fig. 3 shows a comparison between the exact Stokes solution (40) and the force-coupling solution (42) in terms of the streamline pattern for a sphere in a uniform straining flow. The external rate of strain is assumed to be a simple two-dimensional system with $E_{11} = -E_{22} = E$ and all other components zero. The induced stresslet is $G_{11} = -G_{22} = G$ with $G = 20\pi\mu a^3 E/3$. Away from the sphere surface the streamline pattern from the force-coupling result resembles that of the Stokes solution. Fig. 3 also shows that the force-coupling model sets up an recirculating flow creating a fictitious sphere slightly larger than the actual sphere. In Fig. 4 the velocity profiles for the induced stresslet flow fields shown in Fig. 3. The figure shows the profile of the u_1 velocity component as a function of the distance along the x_1-axis and along the line $x_1 = x_2$. The agreement with the exact Stokes solution is again very good for distances $r/a > 1.25$, while close to the sphere the approximate force-coupling result deviates slightly from the exact solution.

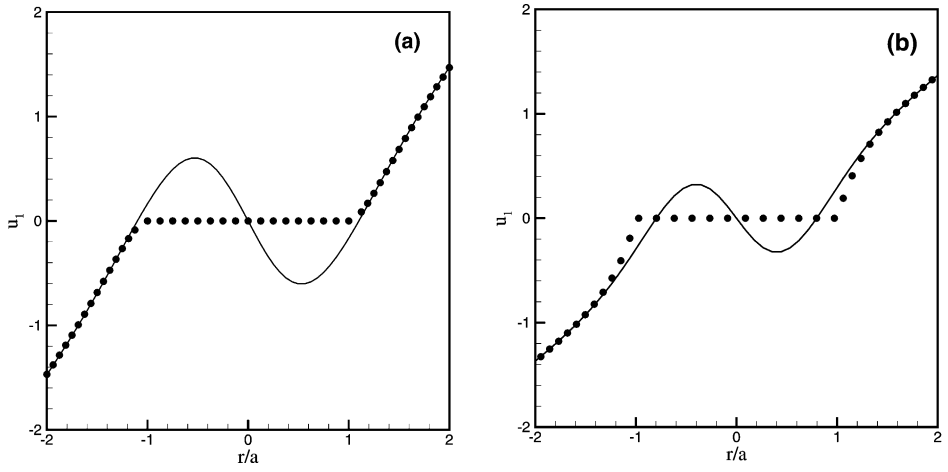

Fig. 4. Profile of the u_1 fluid velocity as function of the distance along the x_1-axis (a) and along the line $x_1 = x_2$ (b) for an isolated sphere of radius a in a uniform straining flow $u_1 = x_1$, $u_2 = -x_2$, and $u_3 = 0$ as given by the force-coupling result (42). The Stokes solution is shown as • and the FCM result as the line.

4. Motion of particle pair

The next case to examine is the steady motion of a pair of isolated equal sized spheres settling under gravity. In this case two different problems may be considered; one where the forces on the spheres are equal in both magnitude and direction, and one where the forces are equal in magnitude but opposite in direction. The results from the force-coupling model will be compared with data taken from Batchelor [25], Batchelor [26], and Ganatos et al. [27] who all presented exact data based on the solutions by Stimson and Jeffery [28].

4.1. Forces in same direction

In the first problem, with the spheres both settling, the mutual influence of the disturbance flow created by each particle leads to a settling velocity larger than that for a single isolated particle. The settling velocity of the pair depends on the separation between the particles and the orientation of the line of centers to the vertical [25]. Once the settling velocity has been determined for the two standard configurations, two spheres separated either vertically or horizontally, the settling velocity is given for all other configurations [25]. However, only for these two basic configurations will the spheres settle vertically.

The results are obtained by numerically evaluating the analytical expressions (19a) to (20b) and (22a) to (23b) for the flow field and computing the integrals for the particle velocity (6), angular velocity (16) and the average rate of strain (17). The pair of particles have a basic symmetry that determines the form of force dipole coefficients; so following a calibration step for a single dipole a simple system of linear equations can be solved to determine the coefficients from (17). The integrals are all convolutions and each integral can be evaluated as a simple Riemann sum over a uniform, three-dimensional grid centered on the particle. The sum yields spectral accuracy provided the grid is large enough and the spacing small enough.

In Fig. 5 the results from the force-coupling model evaluated using only a monopole term and using both a monopole and a dipole term are compared with the theoretical results. When the spheres are separated vertically the force-coupling model with only the monopole gives a qualitatively correct result with an error below 5%. Including the force dipole clearly improves the solution and the error drops to below 1%.

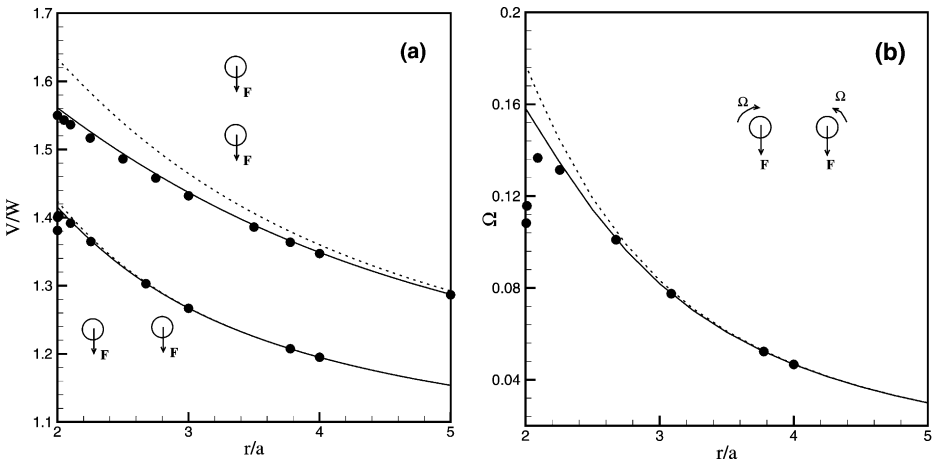

Fig. 5. Comparison of the force-coupling model with the exact Stokes solution for a pair of equal spheres with either vertical separation or horizontal separation. The settling velocities are shown in (a) and the angular velocity in the case of horizontal separation is shown in (b). r/a is the center to center distance between the spheres. (•) Stokes solution; (···) force-coupling solution with only the monopole; (—) force-coupling solution with both force terms.

In the case of the horizontally separated spheres the force-coupling method performs very well and the effect of the force dipole is negligible until very near contact. In this case the spheres will rotate in opposite directions with an angular velocity of the same magnitude. The left sphere will rotate clockwise and the right sphere anti-clockwise. The influence of this on the settling velocity of the pair is a net increase. However, once the spheres come close together the rotation diminishes (to zero at $r/a = 2$) due to the no-slip condition at the sphere surfaces and this causes the theoretical settling velocity to drop for distances $r/a < 2.01$. Since the force-coupling method does not resolve the flow near the surface of the spheres this is not captured by the method. The angular velocity of the spheres is also shown in Fig. 5. The inclusion of the force dipole improves the force-coupling result, but as already mentioned the model cannot fully resolve the flow field when the two spheres are close together $r/a < 2.25$.

The discrepancies for the two problems above are not critical for particle suspensions at low to moderate concentrations. However, for closely packed suspensions they may give rise to errors.

4.2. Forces in opposite direction

When the forces on two equal sized spheres are equal in magnitude but opposite in direction the velocity of each sphere will also be equal in magnitude and opposite in direction. However, since the spheres are moving in opposite directions the absolute value of the particle velocity will be smaller than the corresponding Stokes terminal velocity.

The settling velocities obtained with the force-coupling method are compared with the theoretical values in Fig. 6. For the horizontally separated spheres the force-coupling model does well and the difference between using the force monopole only and including both force terms is negligible. However, when the spheres are separated only vertically including the force dipole results in a much better result with an error of 10% at $r/a = 2.5$, while the error on the monopole result at this point is 28%. Lubrication effects become important in the case of vertical separation and the lack of these effects in the model causes the discrepancies when the two spheres come close together.

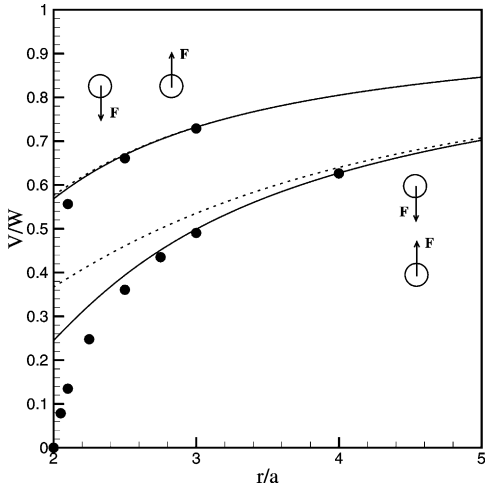

Fig. 6. Comparison of the force-coupling model with the exact Stokes solution for a pair of spheres subject to a force equal in size but opposite in direction. The separation is either vertical or horizontal. r/a is the center to center distance between the spheres. (•) Stokes solution; (···) force-coupling solution with only the monopole; (—) force-coupling solution with both force terms.

5. Sphere in a plane channel

So far the force-coupling model has been examined in various cases of an unbounded domain. In this section the capabilities of the force-coupling model within a simple bounded geometry will be investigated. The setup is a sphere moving in a plane channel as shown in Fig. 7. The following cases will be considered:

1. Sphere translating perpendicular to the walls. $V_2 \neq 0$, $V_1 = \Omega = U = 0$.
2. Sphere translating parallel to the walls. $V_1 \neq 0$, $V_2 = \Omega = U = 0$.
3. Sphere rotating between the walls. $\Omega \neq 0$, $V_1 = V_2 = U = 0$.
4. Sphere rigidly held in a Poiseuille flow. $U \neq 0$, $V_1 = V_2 = \Omega = 0$.

These cases correspond to those computed by Ganatos et al. [29,30]. The results of Ganatos et al. [29,30] were obtained using a boundary-multipole collocation method for solving the same Stokes problem and they are exact in the first three digits. Ganatos et al. [29,30] solved the resistance problem, i.e. they specify a velocity and determine the force and torque on the sphere. In the force-coupling model the mobility problem is solved instead, i.e. a force and a torque is specified and this determines the velocity and angular velocity of the sphere. However, in Stokes flow these two problems are the inverse of each other and therefore a solution from the force-coupling model may be inverted and compared with the accurate solutions by Ganatos et al. [29,30].

5.1. Numerical method

In contrast to the problems in the unbounded domain the plane channel problem has been solved numerically. The full force-coupling equations (1) with $\mathbf{f}(\mathbf{x}, t)$ given by (11) have been solved in a channel with no-slip boundary conditions on the walls and periodic boundary conditions in the two other directions. The original code was obtained from Handler et al. [31] and it uses the Fourier–Chebyshev tau method of Kim et al. [32]. Implementation of the force-coupling terms is described in Lomholt [23] and Lomholt et al. [24]. Since the problems considered here are steady Stokes flow the non-linear terms are set to zero and the time integration is used as an iteration scheme until a constant velocity $\mathbf{V}$ or angular velocity $\mathbf{\Omega}$ of the sphere has been reached. The sphere is not moved, because we want to investigate the effect of the sphere at various given positions in the channel and this requires the sphere to be maintained at its initial position. The resolution was set so that there are at least 4 points in each direction inside the particle and the lengths of

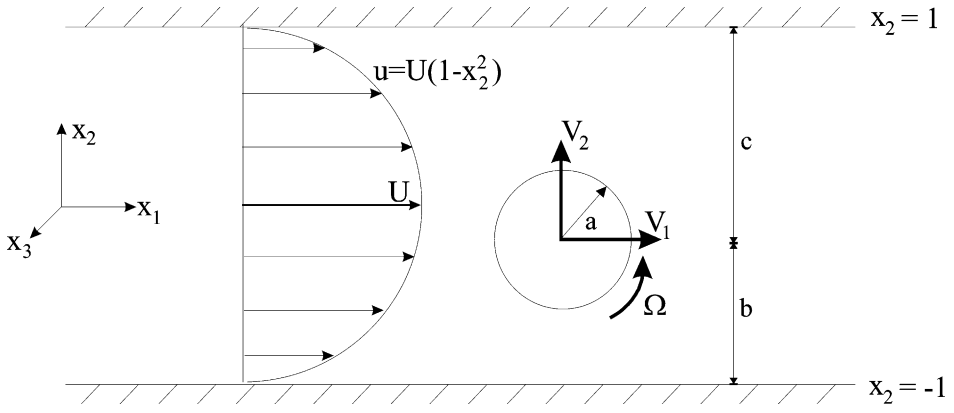

Fig. 7. Geometry for a sphere of radius a placed between two walls at $x_2 = \pm 1$. U is the center line velocity of the parabolic velocity profile u for the Poiseuille flow. V_1 and V_2 are the steady velocity of the sphere in direction x_1 and x_2, respectively. Ω is the steady angular velocity of the sphere around the x_3-axis. b and c are the distance from the sphere center to the bottom and the top wall, respectively.

the periodic directions were $L_1 = L_3 = 24a$, while the length in the wall normal direction was $L_2 = 2$. Increasing the lengths of the two periodic directions beyond $L_1 = L_3 = 24a$ was tested and no change in the results was found. The resolution in these periodic directions was set to $N_1 = N_3 = 32$ in all the computations, while the resolution in the normal direction varied from $N_2 = 16$ for the large sphere in a narrow channel (corresponding to $b/a = 1.1$ and $s = 0.5$ in the figures below) to $N_2 = 144$ for the small sphere in a wide channel (corresponding to $b/a = 5.0$ and $s = 0.05$ in the figures below).

5.2. Sphere translating perpendicular to the walls

The geometry for motion perpendicular to the wall is given in Fig. 7 with $U = 0$, $V_1 = 0$, $\Omega = 0$, and $V_2 > 0$. The drag force on the sphere may be expressed as,

$$F_2^{\mathrm{D}} = -6\pi\mu a V_2 \lambda^t, \tag{45}$$

where λ^t is a correction to the Stokes drag due to the presence of the two confining walls. In the steady state the drag force given by (45) is balanced with the buoyancy force, which is used as the force monopole strength $\mathbf{F}$ in (11). The buoyancy force is

$$F_2^{\mathrm{b}} = \frac{4}{3}\pi a^3(\rho_p - \rho)g_2, \tag{46}$$

where ρ_p is the density of the sphere and $\mathbf{g} = (0, -g, 0)$ is the gravitational acceleration. Balancing (45) with (46) gives

$$\lambda^t = \frac{2}{9}\frac{a^2}{\nu}\frac{g_2}{V_2}\left(\frac{\rho_p}{\rho} - 1\right). \tag{47}$$

Therefore the drag coefficient, λ^t, in our computations is determined from the computed constant velocity V_2 of the sphere. A sphere moving perpendicular to the wall does not rotate and therefore solving this problem does not require a torque.

In Fig. 8(a) the drag coefficient from our computations is compared with the results of Ganatos et al. [29]. The coefficient is shown as a function of the position in the channel given by [1] $s = b/(b + c)$ and the distance to the bottom wall given by the ratio b/a, see Fig. 7. Our results agree well with the exact values when the distance from the wall to the sphere is larger than half the sphere radius ($b/a \geqslant 1.5$). Closer to the wall ($b/a = 1.1$) the drag coefficient from our results agree qualitatively but the values are approximately 17% and 48% smaller for $b/a = 1.25$ and $b/a = 1.1$, respectively. Therefore our model does not capture the full effect of the wall. When the sphere is close to the wall ($b/a \leqslant 2.0$) lubrication effects become important [9] and the lack of lubrication effects in the force-coupling method is the main reason for the discrepancy. The level of accuracy for this sphere-wall problem is consistent with that of the two sphere motion in Fig. 6. The lubrication effects would be included if the force multipole expansion included many more terms, but this is in general impossible and the forces due to the lubrication must be modeled.

In Fig. 8(b) the correction factor computed with both force terms is compared with the correction factor obtained using only the force monopole. In the three cases closest to the wall the dipole clearly improves the solution for $s < 0.4$, but for wall to sphere distances larger than the sphere radius the effect of the dipole is negligible. When the sphere is placed in the center of the channel the dipole term is zero because of the symmetry. The effect of the dipole increases when the sphere is moved closer to the bottom wall (s becomes smaller) and the symmetry is broken.

[1] When $s = 0.5$ the particle is placed in the center of the channel and when $s = 0$ the top wall is "infinitely" far away.

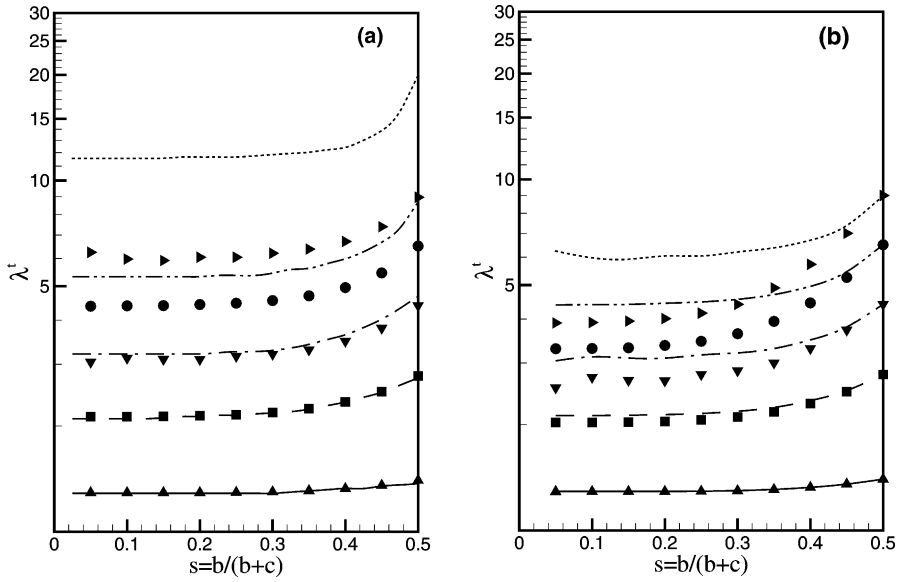

Fig. 8. Results for a sphere translating perpendicular to the walls. (a) shows a comparison of the drag coefficient λ' from the force-coupling model using both force terms (symbols) with the results of Ganatos et al. [29] (lines). (b) shows a comparison of the drag coefficient λ' computed with both force terms (lines) and with only the force monopole (symbols). (▲) and (—) $b/a = 5.0$; (■) and (− − −) $b/a = 2.0$; (▼) and (− · − · −) $b/a = 1.5$; (●) and (− · · − · · −) $b/a = 1.25$; (▶) and (· · ·) $b/a = 1.1$.

A streamline and vector plot for $b/a = 1.5$ and $s = 0.3$ is shown in Fig. 9 for a plane through the center of the sphere. The sphere is shown as the full drawn line and the walls are placed at $x_2 = \pm 1$. The streamlines are in the reference system of the sphere, while the vector plot is in the frame of the channel. The streamlines show that the force-coupling model sets up two recirculation zones creating a fictitious particle slightly larger than the actual sphere. Due to the wall, the fictitious particle has a weak spheroidal form and this causes the discrepancy in the drag coefficient seen in Fig. 8(a). When $b/a = 1.1$ the shape of the fictitious particle is even more spheroidal and hence the discrepancy in Fig. 8(a) between the exact drag coefficient and our result is larger. This means that the dipole included in our model is not enough alone to avoid the particle from deforming, when lubrication forces becomes important. The asymmetry in the streamlines is a result of the squeezing of the fictitious sphere, which causes a small asymmetry in the dipole forcing and therefore also in the velocities. The same asymmetry exist as well in the other periodic direction, i.e. in the x_2–x_3 plane. The vector plot shows that the translation of the sphere generates a ring shaped recirculation zone around the particle, where the flow goes from the top of the sphere to the bottom of the sphere. This is very similar to the vector plot given in Ganatos et al. [29].

5.3. Sphere translating parallel to the walls

The next Stokes problem to be considered is a sphere moving parallel to the plane walls. The geometry for this problem is shown in Fig. 7 with $U = 0$, $V_2 = 0$, and $\Omega = 0$. In the force-coupling model a force and/or torque is specified and the corresponding velocities are then determined with linear relations of the form,

$$V_i = A_{ij}F_j + B_{ij}T_j, \tag{48a}$$

$$\Omega_i = C_{ij}F_j + D_{ij}T_j. \tag{48b}$$

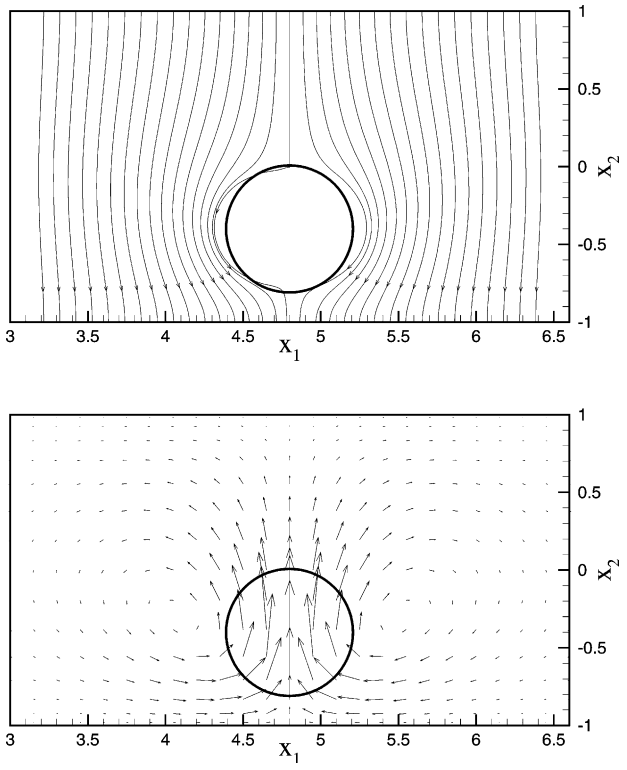

Fig. 9. Streamlines and vector plot for a sphere translating perpendicular to the walls; the walls are placed at $x_2 = \pm 1$; $s = 0.30$, $a = 0.40$, and $b/a = 1.5$.

However, the problem specified here is the inverse namely to determine the force and torque due to a given velocity of the sphere,

$$F_i = A'_{ij} V_j + B'_{ij} \Omega_j, \tag{49a}$$

$$T_i = C'_{ij} V_j + D'_{ij} \Omega_j. \tag{49b}$$

Therefore the drag and torque coefficients in this section have been found by solving the problem (48a) and (48b) first for a given force with zero torque and then for a given torque and zero force. This gives the coefficients A_{ij}, B_{ij}, C_{ij}, and D_{ij} and the problem may be inverted to give a force and a torque due to a velocity and/or an angular velocity. It is worth noting that the force-coupling model preserves the usual reciprocal theorem properties with $B_{ij} = C_{ji}$. In this section only the first case with a velocity and zero angular velocity is considered.

The drag correction factor λ' is defined as in (45) and is computed by evaluating the force determined from (49a) with $\boldsymbol{V} = (V_1, 0, 0)$ and $\boldsymbol{\Omega} = 0$. The results from the force-coupling model, computed using both force terms, are compared with the results from Ganatos et al. [30] in Fig. 10(a). When the distance from the wall to the sphere is greater than half the sphere radius ($b/a \geqslant 1.5$) the results agree reasonably well. The λ' from the force-coupling model is generally smaller than the exact values found by Ganatos et al. [30] with the difference being up to 5%. When the sphere is placed nearer the wall the qualitative discrepancy becomes larger and the errors are approximately 4% and 10%. Close to the wall the discrepancy observed

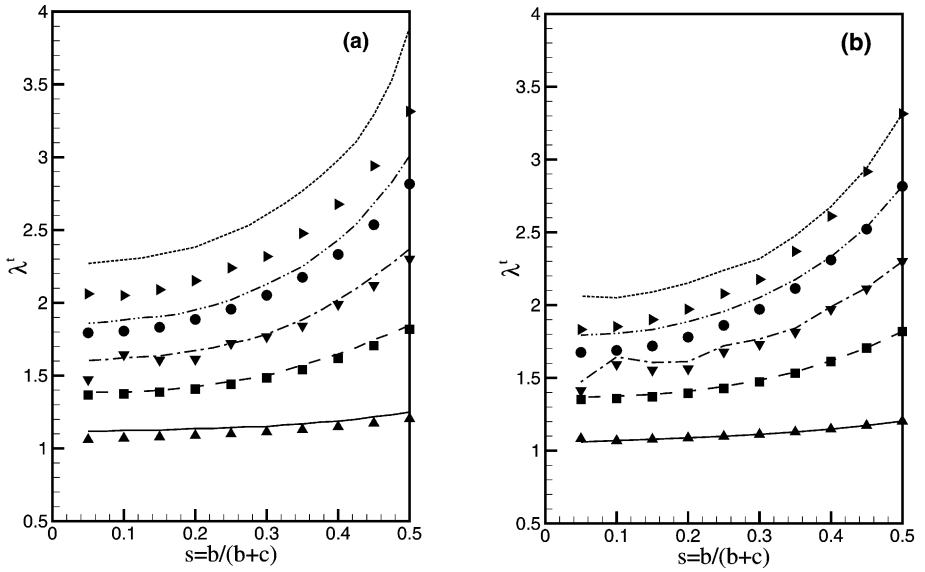

Fig. 10. Results for a sphere translating parallel to the walls. (a) shows a comparison of the drag coefficient λ^t from the force-coupling model using both force terms (symbols) with the results of Ganatos et al. [30] (lines). (b) shows a comparison of the drag coefficient λ^t computed with both force terms (lines) and with only the force monopole (symbols). (▲) and (—) $b/a = 5.0$; (■) and (− − −) $b/a = 2.0$; (▼) and (− · − · −) $b/a = 1.5$; (●) and (− · · − · · −) $b/a = 1.25$; (▶) and (· · ·) $b/a = 1.1$.

for the parallel motion is considerably smaller than it was for the perpendicular motion, because the effect of the wall is not as severe in the case of parallel motion. The reason for the better agreement may be found by considering the forces for a sphere nearly touching the wall. For a sphere translating perpendicular to the wall the lubrication force to the first order is $\mathbf{F}_{\text{lub}} \sim (b/a - 1)^{-1}$, while for the parallel motion it is $\mathbf{F}_{\text{lub}} \sim \ln(b/a - 1)$ to the first order [9]. Thus for a sphere in perpendicular motion the dependency on the distance to the wall is more severe than for a sphere in parallel motion.

Fig. 10(b) presents a comparison of the drag coefficient computed with and without the force dipole. When the distance from the wall to the sphere is larger than the sphere radius ($b/a \geqslant 2$) the results are almost indistinguishable. Closer to the wall on the other hand the results with only the force monopole are clearly smaller and the dipole term becomes important. This is consistent with the results for perpendicular motion; the dipole is only important, when the sphere is within one radius of the wall.

A hydrodynamic torque acts on the sphere as it translates, without rotation, parallel to the plane walls and this torque is balanced by an external torque on the sphere. This external torque is transmitted to the fluid and is equal to the torque $\mathbf{T}$ in (49b) for the force-coupling model, with $\mathbf{V} = (V_1, 0, 0)$ and $\Omega = 0$. In the notation of Gantos et. al [30], the non-zero component of the torque is

$$T_3 = 8\pi\mu a^2 V_1 \lambda_T^t. \tag{50}$$

The results for the torque coefficient λ_T^t from the force-coupling model are compared in Fig. 11(a) with those from Ganatos et al. [30]. When the sphere is close to the wall, and the second wall is far away, there is a slight tendency for the sphere to roll along the wall. This is prevented by the external torque and is evident in the positive values of λ_T^t for smaller values of s. The tendency is reversed if the gap between the particle and the lower wall is larger and the second wall has an influence. Both features are seen in the results from the force-coupling model.

In general, for distances $b/a \geqslant 1.25$ the results agree with Ganatos et al. [30], although the agreement is not as good as for the drag coefficient. One possible reason for this is that the value of λ_T^t is small and

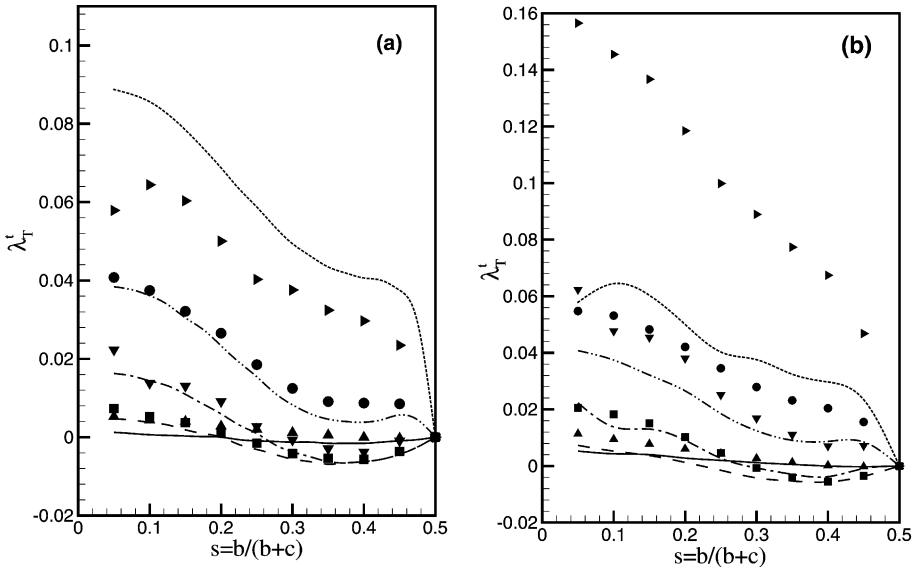

Fig. 11. Results for a sphere translating parallel to the walls. (a) shows a comparison of the torque coefficient λ_T^t from the force-coupling model using both force terms (symbols) with the results of Ganatos et al. [30] (lines). (b) shows a comparison of the torque coefficient λ_T^t computed with both force terms (lines) and with only the force monopole (symbols). (▲) and (—) $b/a = 5.0$; (■) and (− − −) $b/a = 2.0$; (▼) and (− · − · −) $b/a = 1.5$; (●) and (− · · − · · −) $b/a = 1.25$; (▶) and (· · ·) $b/a = 1.1$.

therefore it will be more contaminated by errors in the approximation and the numerical solution than λ^t. Closer to the wall the discrepancy is due to the lack of lubrication effects in our model, as discussed above. In Fig. 11(b) λ_T^t is shown for solutions with and without the force dipole. Clearly the force dipole has a large influence on the rotation and when it is omitted the angular velocity of the sphere is largely overestimated.

Fig. 12 shows a streamline and a vector plot of the flow field in a plane through the center of the sphere for $b/a = 1.5$ and $s = 0.3$. The streamlines are shown in the frame of the sphere, the sphere is the full drawn line and the walls are placed at $x_2 = \pm 1$. Similarly to perpendicular motion the streamline plot shows that the force-coupling sets up recirculation zones around the sphere. This creates a fictitious sphere and due to the wall it is squeezed into a slightly spheroidal form. In the coordinate frame of the channel the vector plot shows that the translating sphere creates a recirculation zone at the wall placed at $x_2 = 1$. Even though the flow is not fully resolved at the sphere boundary a comparison of the vector plot with that given by Ganatos et al. [30] shows that the flow is very similar.

5.4. Sphere rotating between the walls

The problem of a sphere rotating without translation corresponds to Fig. 7 with $U = 0$, $V_1 = 0$, $V_2 = 0$, and $\Omega_3 = \Omega$. An external torque on the sphere is required to maintain the rotation and at the same time an external force on the sphere is required to counteract the tendency of a sphere, close to the wall, to drift in a rolling motion due to the induced flow. The external force and torque on the sphere are equal to those of the force-coupling model and may be written as [30]

$$F_1 = 6\pi\mu a^2 \Omega \lambda^r, \tag{51}$$

$$T_3 = 8\pi\mu a^3 \Omega \lambda_T^r. \tag{52}$$

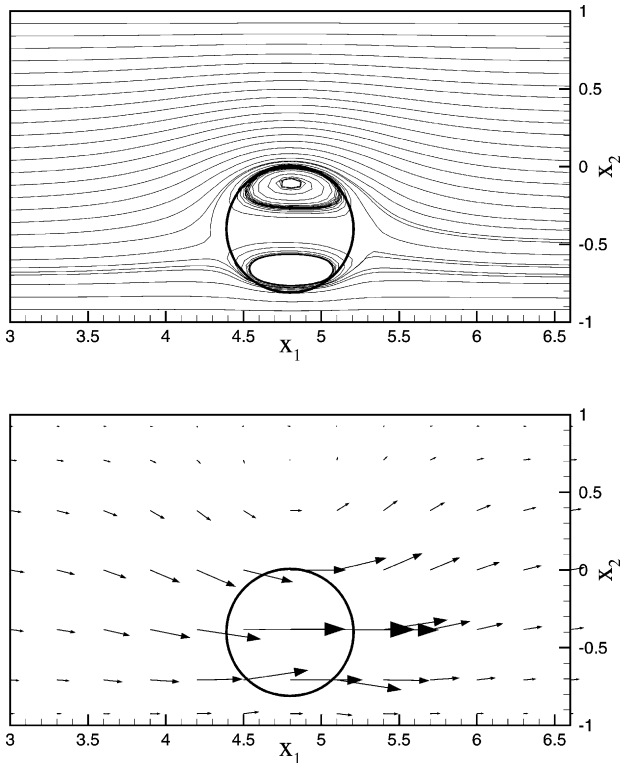

Fig. 12. Streamlines and vector plot for a sphere translating parallel to the walls; the walls are placed at $x_2 = \pm 1$; $s = 0.30$, $a = 0.40$, and $b/a = 1.5$.

The coefficients λ^r and λ^r_T are evaluated from the results ((49a) and (49b)), derived from the force-coupling model.

The results from the rotating sphere are shown in Figs. 13(a) and (b). Fig. 13(a) compares the λ^r from the force-coupling model with the results of Ganatos et al. [30] and the agreement is reasonable. Among the factors contributing to the differences are the lack of lubrication effects and numerical errors in the solution procedure, as already discussed above. The comparison for the torque coefficient λ^r_T is shown in Fig. 13(b) and at distances $b/a \geqslant 1.25$ the agreement is very good. Very close to the wall ($b/a = 1.1$) the quantitative discrepancy is again due to the lack of lubrication effects.

In Fig. 14, a streamline and a vector plot of the flow field through the center of the sphere is shown. The sphere is shown as the full line. The streamline plot in the frame of the sphere shows that the force-coupling method sets up one recirculation zone, unlike the cases with the translating sphere where two recirculation zones were created. Furthermore, it is not possible to distinguish the fictitious sphere from the rest of the flow. The vector plot is given in the coordinate frame of the channel and is very similar to that given by Ganatos et al. [30].

5.5. Sphere rigidly held in a Poiseuille flow

The final example concerns a sphere in a Poiseuille flow. In order to compare with Ganatos et al. [30] the sphere must be rigidly held, that is the sphere is not allowed to move. The setup is shown in Fig. 7 with $V_1 = 0$, $V_2 = 0$, $\Omega = 0$, and $\mathbf{U} = (U, 0, 0)$. Solving this problem with the force-coupling model is similar to

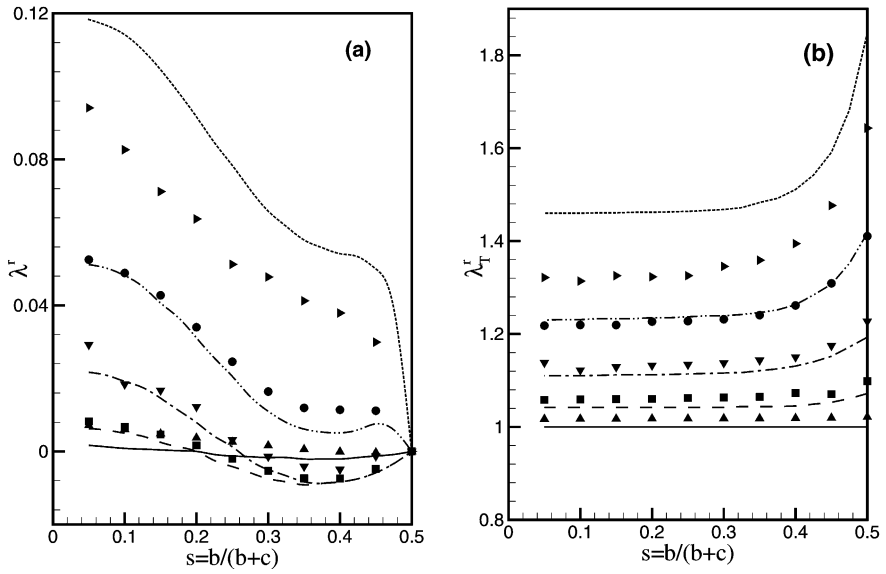

Fig. 13. Results for a steady rotating sphere. Comparison of the drag coefficient λ^r (a) and the torque coefficient λ_T^r (b) from the force-coupling model using both force terms (symbols) with the results of Ganatos et al. [30] (lines). (▲) and (—) $b/a = 5.0$; (■) and (– – –) $b/a = 2.0$; (▼) and (– · – · –) $b/a = 1.5$; (●) and (– · · – · · –) $b/a = 1.25$; (▶) and (· · ·) $b/a = 1.1$.

solving the case of a translating or rotating sphere in Eqs. (48a) and (48b). However, in the case of a Poiseuille flow there is an additional term related to the external Poiseuille flow, so the equations for this case are

$$V_i = A_{ij}F_j + B_{ij}T_j + V_i^{\text{Pois}}, \tag{53}$$

$$\Omega_i = C_{ij}F_j + D_{ij}T_j + \Omega_i^{\text{Pois}}, \tag{54b}$$

where V_i^{Pois} and Ω_i^{Pois} are the velocity and angular velocity of the spheres when no force and no torque are applied. Using the force-coupling model the problem is then solved in three separate steps. One with a specified force and no torque, one with a specified torque and no force, and one without any force or torque. This gives the coefficients A_{ij}, B_{ij}, C_{ij}, and D_{ij} and the velocities V_i^{Pois} and Ω_i^{Pois}, from which the problem may be inverted to find the necessary force and torque to hold the sphere fixed in the Poiseuille flow. The force is then written as

$$F_1^P = 6\pi\mu a U\lambda^P \ , \tag{55}$$

to find the non-dimensional drag coefficient λ^P [30]. The torque is balanced with

$$T_3 = 8\pi\mu a^2 U\lambda_T^P \ , \tag{56}$$

to find the corresponding torque coefficient λ_T^P [30].

The correction factor λ^P from the force-coupling model is compared with those obtained by Ganatos et al. [30] in Fig. 15(a). In contrast to the results above for the translating or rotating sphere, the λ from our computation is in excellent agreement for all values of b/a. Similarly the results for the torque coefficient λ_T^P shown in Fig. 15(b) agrees very well with the values from Ganatos et al. [30].

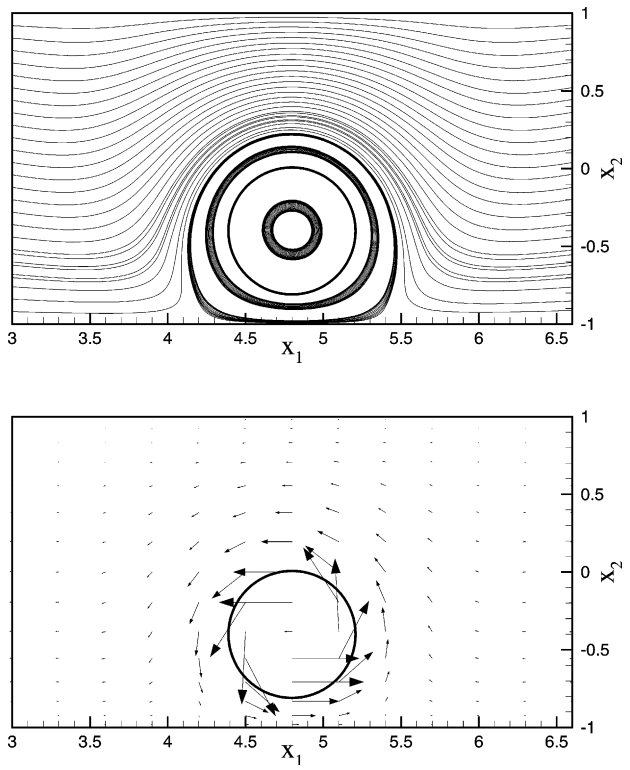

Fig. 14. Streamlines and vector plot for a sphere in rotating motion; the walls are placed at $x_2 = \pm 1$; $s = 0.30$, $a = 0.40$, and $b/a = 1.5$.

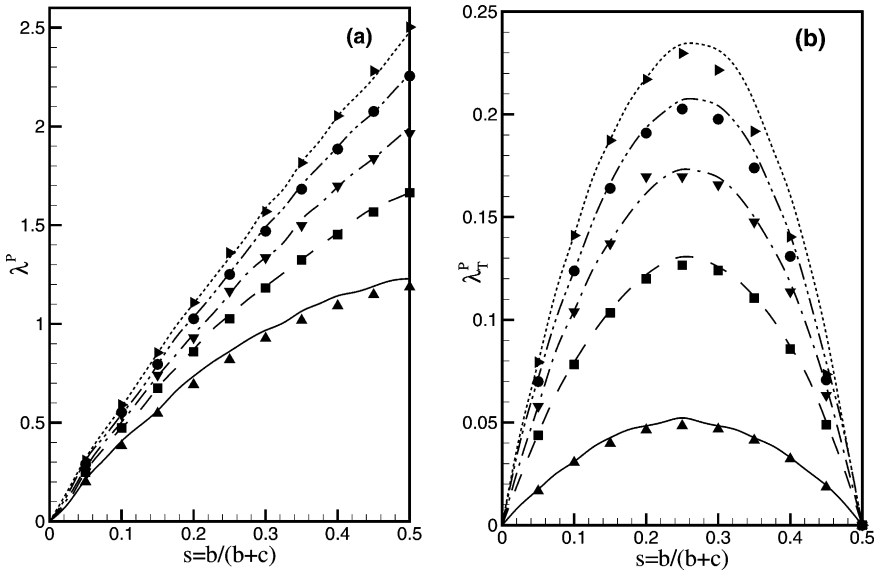

Fig. 15. Results for sphere rigidly held in a Poiseuille flow. Comparison of the drag coefficient λ^p (a) and the torque coefficient λ_T^p (b) from the force-coupling model using both force terms (symbols) with the results of Ganatos et al. [30] (lines). (▲) and (—) $b/a = 5.0$; (■) and (– – –) $b/a = 2.0$; (▼) and (– · – · –) $b/a = 1.5$; (●) and (– · · – · · –) $b/a = 1.25$; (▶) and (· · ·) $b/a = 1.1$.

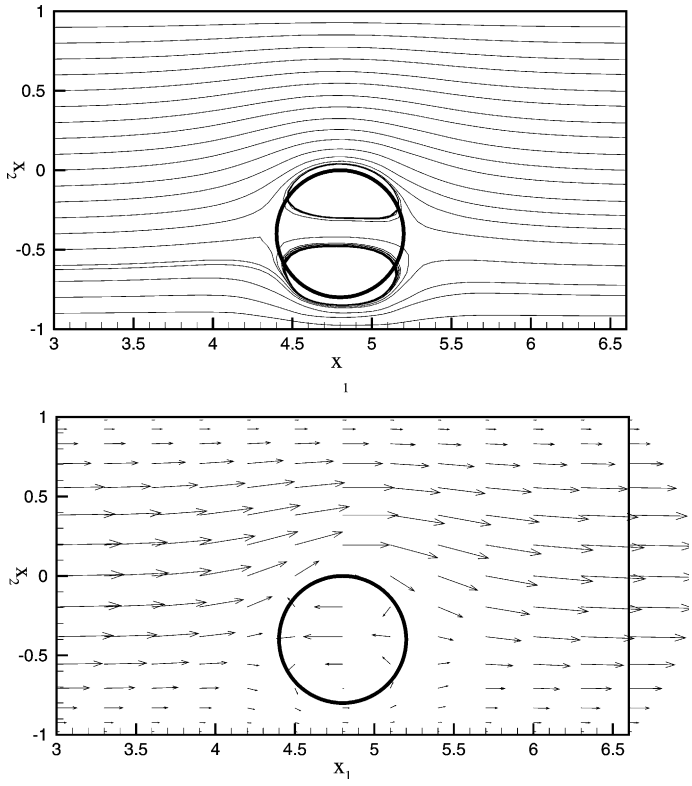

Fig. 16. Streamlines and vector plot for a sphere in a Poiseuille flow; the walls are placed at $x_2 = \pm 1$; $s = 0.30$, $a = 0.40$, and $b/a = 1.5$.

A streamline and a vector plot of the flow field for $b/a = 1.5$ and $s = 0.3$ are shown in Fig. 16. The streamlines are similar to those seen in Fig. 12 for the sphere moving parallel to the walls. However, the fictitious sphere in Fig. 16 does not seem to be squeezed and the shape is more spherical. In the vector plot it becomes very obvious that the flow goes around the sphere, deflected towards the upper part of the channel. Furthermore, it can be seen that the force-coupling model sets up an internal flow that opposes the external Poiseuille flow. The particle velocity, determined from the integral (6), is a combination of the internal flow and the local external flow and is zero overall.

6. Discussion

In this paper we have described the force-coupling method for computing particle dynamics in fluid flows, extending the initial formulation based on monopole terms to include force dipoles too. The model is developed in the context of Stokes flow. Comparison with analytical results for a single sphere and a pair of spheres in an unbounded domain showed that for distances larger than a quarter of a radius away from the sphere surface the flow is accurately represented, except for the case of two spheres moving opposite to each other on the same vertical line. The reason is the lack of lubrication forces here in the force-coupling description for particles in close proximity. Furthermore, it should be

emphasized that the parameters in the model are determined such that the kinetic energy budget is self-consistent.

The method was also tested several cases of Stokes flow in a channel and compared with the results of Ganatos et al. [29,30]. The results similarly showed good agreement when the distance from the wall to the sphere was larger than 25% of the sphere radius. Closer to the wall the lack of lubrication forces again results in quantitative errors, up to 48% for the worst case, but qualitatively the results still agree. In order to represent the wall correctly the lubrication effects need to be included. One approach is to include more, higher-order force multipoles, but to represent the lubrication effects correctly many terms are needed and this is not feasible. Another approach is to model the lubrication forces as separate short-range forces between pairs of particles, or between a particle and a rigid wall, similar to the procedures adopted in Stokesian dynamics [6]. This has been the subject of recent work by Dance [33].

As noted previously the FCM scheme is applicable to both Stokes flows and finite Reynolds number flows, and can be implemented with standard computational flow-solvers for the Navier–Stokes equations in arbitrary flow geometries. The first step in a numerical solution is to set up a three-dimensional grid for the flow domain, as in the channel flow computations described in section 5 and in Lomholt et al. [24]. Regardless of the number of particles included, there is a fixed overhead for the computation of the base flow. The computation times for the construction of the localized body force $\mathbf{f}(\mathbf{x}, t)$ for the particles and the evaluation of the particle velocities from the flow scale linearly with N, the number of particles. The force monopole terms may be specified explicitly in terms of the applied external body forces on each particle, particle–particle contact forces and particle inertia. The inclusion of contact forces, while scaling in principle with N^2, can be handled efficiently by standard procedures from molecular dynamics, see Dance [33]. We have found in ongoing work that in channel flows with 2000 particles the additional computation time for the particle phase is less than 5% of the overall time when using just the force monopole terms. For larger numbers of particles the costs are still modest and depend more on the efficiency of the computational code.

The stresslet coefficients in (11) are set in order to ensure that the condition (17) on the rate of strain at each particle location is satisfied. This may be solved in general by an iterative procedure, specifying initially a stresslet for each particle based on either the value from the last time-step or the stresslet of an isolated particle in Stokes flow and the current local rate of strain, as in (41). Each iteration requires a reevaluation of the flow to determine the new rate of strain, from which a correction to the stresslet is made. For the calculations presented in section 5, typically 3–5 iterations were made using this simple approach. We find that in practice reducing the locally averaged rate of strain (17) to 1% or less of the ambient value gives excellent overall results for the flow and particle motion. At finite Reynolds number, the convergence reported by Lomholt et al. [24] is slower; a more efficient iteration procedure is given by Dance [33].

Another factor in determining the computational efficiency is the numerical resolution and the size of the numerical grid. These are specified first by the underlying flow geometry and the flow Reynolds number. Relative to this, 4–6 grid points to a particle diameter on a uniform mesh are sufficient to provide accurate numerical resolution. This is significantly lower resolution than is needed for many other schemes and FCM is efficient for determining the motion of small particles in a flow. A larger particle will occupy a larger fraction of the flow domain and higher resolution would be available to consider other schemes.

Acknowledgements

The authors would like to thank R. Handler for providing the original channel code used for the simulation presented in this paper. S. Lomholt would like to thank Risø National Laboratory and UNIC

the Danish Computing Centre for Research and Education for their financial support. M. Maxey wishes to acknowledge support from the National Center for Microgravity Research, Independent Studies Program (award USRA 4500-03). Additional support has been provided by DARPA-ATO under contract No. MDA972-01-C-0024. Furthermore, the authors would like to thank Sarah Dance at Brown University for her comments.

References

[1] C.-M. Ho, Y.-C. Tai, Micro-electro-mechanical-systems (MEMS) and fluid flows, Ann. Rev. Fluid Mech. 12 (1998) 579–612.
[2] S. Lomhol, J.-P. Lynov, P. Telleman, Numerical simulation of magnetic separation of particles in a rectangular microchannel, in: D.J. Harrison, A. van den Berg (Eds.), Micro Total Analysis Systems'98, Kluwer Academic Publishers, Dordrecht, 1998, pp. 419–422.
[3] M.R. Maxey, J.J. Riley, Equation of motion for a small rigid sphere in a non-uniform flow, Phys. Fluid 26 (4) (1983) 883–889.
[4] P.M. Lovalenti, J.F. Brady, The temporal behaviour of the hydrodynamic force on a body in response to an abrupt change in velocity at small but finite Reynolds number, J. Fluid Mech. 293 (1995) 35–46.
[5] C.J. Lawrence, R. Mei, Long-time behaviour of the drag on a body in impulsive motion, J. Fluid Mech. 283 (1995) 307–327.
[6] J.F. Brady, G. Bossis, Stokesian dynamics, Ann. Rev. Fluid Mech. 20 (1988) 111–157.
[7] J. Happel, H. Brenner, Low Reynolds Number Hydrodynamics, Prentice-Hall, Englewood Cliffs, NJ, 1965.
[8] P. Mazur, W. Van Saarloos, Many-sphere hydrodynamic interactions and mobilities in a suspension, Physica A 115 (1982) 21–57.
[9] S. Kim, S.J. Karrila, Microhydrodynamics: Principles and Selected Applications, Butterworth–Heinemann, London, 1991.
[10] A.J.C. Ladd, Hydrodynamic interactions in a suspension of spherical particles, J. Chem. Phys. 88 (1988) 5051–5063.
[11] A.J.C. Ladd, Dynamical simulations of sedimenting spheres, Phys. Fluids A 5 (1993) 299–310.
[12] A. Sangani, G. Mo, An O(N) algorithm for Stokes and Laplace interactions of particles, Phys. Fluids 8 (1996) 1990–2010.
[13] K. Ichiki, J.F. Brady, Many-body effects and matrix inversion in low-Reynolds-number hydrodynamics, Phys. Fluids 13 (2001) 350–353.
[14] A. Sierou, J.F. Brady, Accelerated Stokesian dynamics simulations, J. Fluid Mech. 448 (2001) 115–146.
[15] H.H. Hu, Direct simulation of flows of solid-liquid mixtures, Int. J. Multiphase Flow 22 (1996) 335–352.
[16] A.A. Johnson, T.E. Tezduyar, Simulation of multiple spheres falling in a liquid-filled tube, Comput. Meth. Appl. Mech. Eng. 134 (1996) 351–373.
[17] R. Glowinski, T.W. Pan, T.I. Hesla, D.D. Joseph, A distributed Lagrange multiplier/fictitious domain method for particulate flows, Int. J. Multiphase Flow 25 (1999) 755–794.
[18] N.A. Patankar, P. Singh, D.D. Joseph, R. Glowinski, T.-W. Pan, A new formulation of the distributed Lagrange multiplier/fictitious domain method for particulate flows, Int. J. Multiphase Flow 26 (2000) 1509–1524.
[19] S.O. Unverdi, G. Tryggvason, A front-tracking method for viscous, incompressible, multi-fluid flows, J. Comput. Phys. 100 (1992) 25–37.
[20] M.R. Maxey, B.K. Patel, E.J. Chang, L.-P. Wang, Simulations of dispersed turbulent mulitphase flow, Fluid Dyn. Res. 20 (1997) 143–156.
[21] M.R. Maxey, B.K. Patel, Localized force representations for particles sedimenting in stokes flow, Int. J. Multiphase Flow 27 (2001) 1603–1626.
[22] G.L. Dent, Aspects of particle sedimentation in dilute flows at finite Reynolds numbers, Ph.D. Thesis, Brown University, Providence, RI, 1999.
[23] S. Lomholt, Numerical investigations of macroscopic particle dynamics in microflows, Ph.D. Thesis, Risø National Laboratory, Roskilde, Denmark, 2000.
[24] S. Lomholt, B. Stenum, M.R. Maxey, Experimental verification of the force-coupling method for particulate flows, Int. J. Multiphase Flow 28 (2001) 225–246.
[25] G.K. Batchelor, Sedimentation in a dilute dispersion of spheres, J. Fluid Mech. 52 (1972) 245–268.
[26] G.K. Batchelor, Brownian diffusion of particles with hydrodynamic interaction, J. Fluid Mech. 74 (1976) 1–29.
[27] P. Ganatos, R. Pfeffer, S. Weinbaum, A numerical-solution technique for three-dimensional Stokes flows, with application to the motion of strongly interacting spheres in a plane, J. Fluid Mech. 84 (1978) 79–111.
[28] M. Stimson, G.B. Jeffery, The motion of two spheres in a viscous fluid, Proc. R. Soc. A 111 (1926) 110–116.
[29] P. Ganatos, S. Weinbaum, R. Pfeffer, A strong interaction theory for the creeping motion of a sphere between plane parallel boundaries. Part 1. Perpendicular motion, J. Fluid Mech. 99 (1980a) 739–753.
[30] P. Ganatos, S. Weinbaum, R. Pfeffer, A strong interaction theory for the creeping motion of a sphere between plane parallel boundaries. Part 2. Parallel motion, J. Fluid Mech. 99 (1980b) 755–783.

[31] R.A. Handler, E. Levich, L. Sirovich, Drag reduction in turbulent channel flow by phase randomization, Phys. Fluids A 5 (3) (1993) 686–694.
[32] J. Kim, P. Moin, R. Moser, Turbulence statistics in fully developed channel flow at low reynolds number, J. Fluid Mech. 177 (1987) 133–166.
[33] S.L. Dance, Particle sedimentation in viscous fluids, Ph.D. Thesis, Brown University, 2002.